Journal of Materials Science: Materials in Electronics (2020) 31:9835–9845
https://doi.org/10.1007/s10854-020-03528-y

Novel method to synthesis ZnO nanostructures via irradiation zinc acetate with a nanosecond laser for photocatalytic applications

Noor J. Ridha[1] · Firas K. Mohamad Alosfur[2,3] · Hiba Basim Abbas Kadhim[1] · Lazem H. Aboud[4] · N. Al-Dahan[1,3]

Received: 7 February 2020 / Accepted: 1 May 2020 / Published online: 11 May 2020

Abstract
In this study, a novel method to prepare ZnO nanostructures was proposed by irradiation zinc acetate with nanosecond laser in a liquid medium. Nd-YAG laser was used with energy of 180 mJ and 6000 pulses. As well as, the effects of using various liquids such as ethanol, deionized water, and ethylene glycol on the properties of the prepared ZnO were investigated. Structural, morphological, and optical properties were studied for all samples. Specifically, the X-ray diffractometer results revealed the presence of ZnO with hexagonal crystallization. Most importantly, as indicated by micrographs of scanning electron microscopy, the laser irradiation caused the immediate growth of ZnO nanorods in aqueous solution on the contrary of nanospheres which were grown in the other used solutions. Notably, the optical properties of the prepared ZnO showed that the highest absorption was obtained by ZnO nanospheres. Meanwhile, the energy gap was also studied and found to be between 3.5 and 3.59 eV. The incorporation of all these investigations provides a clear vision for growth mechanisms. This mechanism revealed the one-step growth of ZnO nanostructures with interesting properties that prepared by laser irradiation method. The splendid properties of nanorods structures enhance the photocatalytic performance of ZnO rather than spherical structures. The photocatalyst results revealed that the maximum decomposition of 5 ppm MB by the ZnO nanorods was greater than 98% which achieved after 40 min under UV light irradiation with a fixed catalyst concentration of 12 mg / L.

1 Introduction

Water is one of the most important elements for sustaining life on the earth [1]. It covers two-thirds of the Earth's surface and it presents 75% of the human body. Unfortunately, the water exposes to pollution, due to the dumping wastes from various industrial activities such as tanning, textiles, paper, paints, hair dyes, and cosmetics where (10 to 15%) of the dye is lost in the effluent [2]. Therefore, water systems are contaminated by leakage of harmful wastewater [3, 4]. These effluents flow heavily in the rivers down to the seas and oceans [5]. Finally, they interrupt the beauty of the environment, shade the sunlight, and cause toxicity to marine life [6]. As a result, they cause problems that affect people's lives due to many diseases including cancer. Unfortunately, these dyes are mostly insoluble in water [7]. Among various synthetic dyes, methylene blue (MB) has attracted consideration due to its use in coloring, fabrics, and in painting productions. It is worth to mention that MB is a heterocyclic aromatic compound, toxic, unsafe, and affects human health such as hyperhidrosis, risks of respiration, vomiting, and mental disorders [8, 9].

Therefore, based on these problems, it is required to treat and separate the dyes before dispose them into the rivers [10–12]. One of the novel techniques is the Advanced Oxidation Process (AOP), which is based on the production of reactive types such as hydroxyl radicals ($OH^{\bullet}$) [13, 14]. These radicals oxidize a large group of organic pollutants rapidly and non-selectively [15]. This process involves generating hydroxyl radicals (OH•) in the presence of photons with assistances of catalysts which is able to oxidize the organic dye contamination [16, 17]. In order to apply the process for large volume applications, many parameters have to be considered. These parameters includes the environment temperature and pH, the catalysts' dose, and types

✉ Noor J. Ridha
nooraboalhab@yahoo.com; noor.jawad@uokerbala.edu.iq

1 Department of Physics, College of Science, University of Kerbala, Kerbala, Iraq

2 Department of Environmental Health, College of Applied Medical Sciences, University of Kerbala, Kerbala, Iraq

3 Faculty of Dentistry, University of Alkafeel, Najaf, Iraq

4 Laser Physics Department, Faculty of Science for Women, University of Babylon, Babylon, Iraq

of catalysts [18]. Many researchers studied the effects of these parameters on the photodegradation processes. It was adopted that as the temperature of the system elevated, the photocatalytic properties enhanced due to change in activation energies. As well as, the pH of the environment dramatically effects the properties of both dye and catalyst, which could be attributed to the creation of hydroxyl radical [19]. In addition, low degradation activity can be obtained at low pH. This could be ascribed to the high concentration of produced protons which reduce the degradation. Furthermore, it was revealed that the degradation reduced with the initial dye concentration amount [20].

Metal oxide (MO) semiconductors such as TiO_2 [21–23], SnO_2 [24], Al_2O_3 [25], and ZnO [26] have promising properties to be utilized in many fields such as solar cell, gas sensor, and light emitting diode (LED) [27, 28]. Recently, semiconductors such as ZnO have attracted interest due to their good performance in photocatalyst activity, high electrical conductivity, high stability, inexpensive, and non-toxic properties [29]. As well as, ZnO is a widely used due to its large energy gap (3.37 eV), high exciton binding energy (60 meV), and high resistance to acids and bases [30–33].

Several methods were used to synthesize ZnO nanostructures. These methods could be either top down or bottom up. One of the top down process is the laser ablation in liquid method (LAL), in which the Zn metal plate is placed in the bottom of a glass vessel filled with liquid and is ablated by laser [34]. In our previous work, ZnO pellet was used as a target to be ablated by Nd:YAG laser [35]. Meanwhile, bottom up approach was used to prepare ZnO nanoparticles by irradiation with several sources such as gamma ray [36], visible light [37] and microwave method [38, 39]. Recently, laser was used to irradiate several metals salt such as silver nitrate to prepare silver nanoparticles [40]. In fact, to the best of our knowledge, there is no overview on the synthesis of ZnO nanoparticles by irradiation zinc salts (as a precursor) using laser in liquids. Therefore, we have suggested a novel method to prepare ZnO nanoparticles using available salts namely zinc acetate, which is considered to be inexpensive and suitable for preparation.

In this framework, the main objective is to intensively investigate the conditions of the proposed innovative method by utilizing the Q-Switched nanosecond Nd - YAG laser to irradiate zinc acetate in liquid for preparation ZnO nanoparticles and applied as a photocatalysts. Further aim that will be considered in this study is the feature of utilizing several liquids including (Di water, ethanol, and ethylene glycol) as a liquid media for the preparation in terms of structural, morphological, and optical properties. Next, we can realize the importance of using the prepared ZnO nanoparticles as a catalyst in advanced oxidation process for treating wastewater, specifically regarding elimination of unwanted pollutants. Subsequent, the mechanism of the photodegradation process was also proposed. Finally, future viewpoints related to this preparation method will be investigated taking into account the wastewater treatment applications.

2 Experimental

In this work, novel method was proposed to synthesis ZnO nanostructures, where laser was used to irradiate the zinc acetate in solutions. To control the morphology and other properties of the prepared ZnO, various solvents were used. As well the prepared ZnO was used as a photocatalyst for degradation of methylene blue (MB).

The ZnO nanostructures were prepared via laser irradiation in liquid method. The zinc acetate dihydrate ($Zn(CH_3COO)_2 \cdot 2H_2O$) solution was used as the precursor of zinc ions. All chemicals were purchased from Fluka with high purity (99.5%). The first step of preparation was to dissolve (3 g) of zinc acetate dehydrate in (10 ml) of various solvents (deionized water, ethanol, and ethylene glycol) which were named as DIZn, EthZn, and EGZn, respectively. Vigorous stirring was used to ensure all the chemicals were dissolved well.

Each sample was poured in a glass vessel with continues stirring then irradiated with a laser which was located vertically above the sample. The irradiation process was taking place by Q-Switched nanosecond Nd - YAG laser which has the following parameters: wavelength of 532 nm (2nd harmonic), the energy of 180 mJ/pulse, and repetition rate of 10 Hz. The duration of the laser pulse is about 10 ns with power density of 114.59 W/cm^2. The focused spot diameter of the laser is 2 mm which was focused by the convex lens of (30 cm) focal length. Further details on the system and the preparation conditions can be found in our previous work [41].

After around 20 min, a milky colloidal solution appeared due to nanoparticle creation. The irradiation procedures were taking place alternately since it stopped every 30 s. The samples were irradiated with 6000 laser pulses for 30 min. After the samples were prepared, white precipitations were noticed at the bottom of the flask. These precipitations were separated from the liquid by centrifuge. The collected powder was washed (5 times) with ethanol and another (5 times) with DI water to separate the residual salts (acetate) from the nanoparticles. The samples were then dried using an oven at (100 °C). After drying the samples, the annealing process was applied at (350 °C) to enhance the crystallization of the samples. This synthesis procedure was modified from the basis of the previous works reported by Brito [42] and pyatenko [43]. Nevertheless, the irradiation of zinc acetate by laser in liquids was not reported yet.

The prepared powder was examined by several technics including XRD, SEM, and UV-Vis spectroscopy. To

investigate the structural properties of the samples, the X-ray diffractometer model (6000 Shimadzu Japan) was used. The radiation source of the instrument is Cu Kα with a wavelength ($\lambda = 1.5406$ Å). The system voltage, current, and scan speed were (40.0 Kv), (30.0 mA), and (8.0000 deg/min), respectively. The scanning electron microscopy (SEM) model (Inspect S50) was used to monitor the morphology of the samples. The optical properties were measured using UV/Vis spectroscopy model (CECIL CE 7200 England) with wavelength range (190–1100 nm).

The prepared powder was used as a photocatalyst in the degradation of the methylene blue (MB) dye. The activity of ZnO as a photocatalyst for the degradation of the MB was tested using homemade system, according to previous work [44]. It consisted of the dark box, glass reactor, magnetic bar, magnetic stirrer, fan, and UV light. The UV light (Philips 250 W, high-pressure mercury lamp, Germany) with an intensity of 141.7 W/m^2. The irradiation process was applied for 40 min. The light source was located at (49 cm) height from the surface of the sample. The photoreactor is the main part of the equipment. A glass baker was used as a reactor. The outer part of the reactor is covered well with aluminum foil to prevent light transmission to the sample. The entire system is placed in a dark box. The photocatalyst set-up is demonstrated in Fig. 1.

To prepare (5 ppm) of the MB dye stock (simulated wastewater), (2.5 mg) of the dye was dissolved in (500 ml) of deionized water (DI) and kept in dark place. To dilute this solution, (40 ml) of the MB stock solution was poured into the reactor baker. Then, (12 mg) of ZnO was ultrasonically dissolved in the diluted stock solution for (5 min). The diluted solution was placed in a dark place for (20 min) for adsorption processes. During the experiment, vigorous stirring was continuously applied to prevent MB precipitation at the bottom of the reactor. A proper amount (2 ml) of the solution was pulled out and then examined by UV/Vis spectroscopy. The solution was then irradiated with ultraviolet light. After irradiation, (2 ml) of the solution was pulled out every (10 min) and tested by UV-Vis spectroscopy until the dye was completely degraded and the light became more permeable.

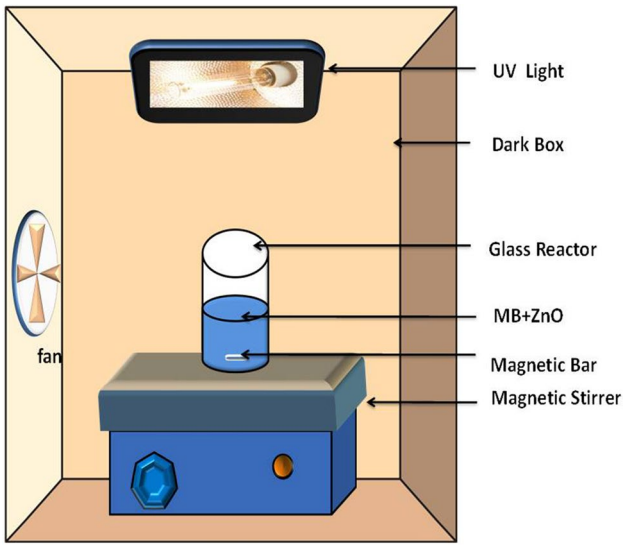

Fig. 1 The handmade photocatalytic set-up

3 Results and discussion

Three samples, namely DIZn, EthZn, and EGZn, were prepared via laser irradiation in different solvents using 180 mJ and 6000 pulses. The structural, morphological, and optical properties of samples were examined after the annealing process. As well as the application of the samples as photocatalysts for MB degradation was lastly tested.

3.1 XRD analysis

Figure 2 represents the XRD spectra of samples DIZn, EthZn, and EGZn. The qualitative research was executed by matching the diffraction peaks of the samples with the ICDD PDF database. This experiment proved that all samples are crystallized in the wurtzite phase of ZnO (hexagonal, P63mc) which matches well with the standard XRD data file of ZnO (JCPDS 00-036-1451). Also, the XRD spectra of both samples EthZn and EGZn show the presence of other peaks which do not match the ZnO peaks, while corresponding to a mineral Zn (ICDD card-00-004-0831). It is clear that sample DIZn is pure ZnO, thus the absence of Zn is due to the high oxidation potential of water. Nevertheless, the high-quality structures could be attributed to the interactions of

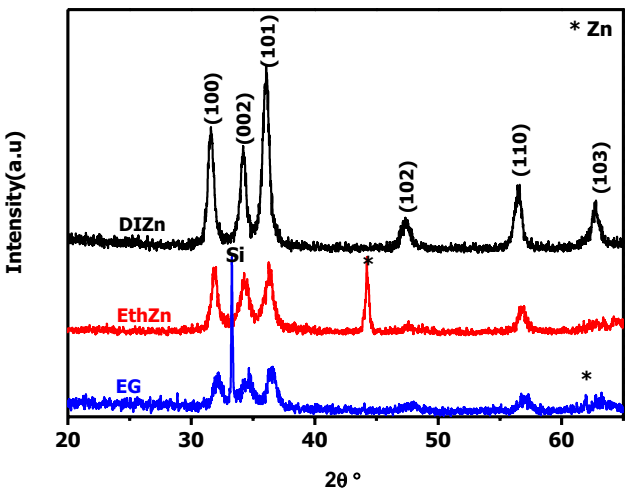

Fig. 2 The XRD spectra of ZnO prepared by LAL of different solvent at 6000 pulses and 180 mJ

Zn acetate with different solvents which become faster in the presence of high-speed laser pulses. Hence, these solvents (ethanol and ethylene glycol) have low oxidation potential; thus, the synthesized materials contain both Zn and ZnO. As well, it is clear from the XRD spectra that the strongest relative intensities of the ZnO peaks are at approximately $2\theta = 36°$, which proves that the preferred orientation of all three samples is the (101) plane. The appearance of Si peak in the XRD pattern is due to the substrate where Si wafer was used for SEM characterization. It was reported in previous work that the metallic zinc was regularly obtained when ZnO nanoparticles were prepared using the LAL method. This is due to insufficient oxygen during the LAL process in organic solvents and DI water. The preferred peak of sample DIZn is (101) at the angle (36.05°), while the preferred peak of sample EthZn is (101) at the angle (36°) and the preferred peak of sample EGZn is (36.65°). The wide FWHM indicates that the prepared samples have a small size. It is observed that the average crystal size of sample DIZn is (20.69 nm), EthZn is (60.87 nm), and EGZn is (61.91). The crystal size of sample DIZn is the smallest compared with EthZn and EGZn. This could be attributed to the dependency of the solubility of zinc acetate ($Zn(CH_3COO)_2{\cdot}2H_2O$) on the nature of the solvents. Thus, the zinc acetate can dissolve easier and faster in DI water rather than other surfactants (ethanol and ethylene glycol). Therefore, solubility plays an essential rule to reduce the size of nanocrystallites. Hence when laser pulses hit the solution, the chemical reactions started to produce small ZnO nanoparticles.

3.2 SEM analysis

Figure 3 reveals the morphology of the samples DIZn, EthZn, and EGZn examined by SEM. Each micrograph contained low and high magnification to examine the morphology of the samples. The microscopic images observed in Fig. 3a related to sample DIZn prove the formation of hexagonal rods. From the high-resolution image Fig. 3d, the nanorods originally growth from small nanoparticles between ~ 20 and ~ 30 nm ± 3 nm as shown in the schematic diagram in Fig. 3g. By comparison of these results with previous work which was prepared by LAL using water as liquid media, we can found that the morphology and sizes are in the good agreement since rod-shaped ZnO was also obtained. It was reported that the usage of DI- water as a liquid media will produce ZnO nanorods. The suggested growth mechanism revealed that the DI water was captured on the (001)/(00$\bar{1}$) polar facets of pure ZnO, which encouraged the growth in 101 directions to form one dimension (1D) structures. The high intensity of (101) of sample DIZn reported in XRD results is an indicator of the growth in 1D.

The morphology of the sample EthZn prepared in ethanol shown in Fig. 3b. The microscopic images of ZnO nanostructures demonstrate the formation of microspherical structures of approximately 500–800 nm in diameter. Small nanoparticles of around ~ 40 to ~ 60 ± 3 nm aggregated together to form larger microspherical structures as shown in high magnification Fig. 3e. Each microsphere contains several nanoporous inside it which separates the nanocrystallites among each other. As well, these microspheres are separated by microporous as represented in the diagram in Fig. 3h. The aggregation of synthesized ZnO nanostructures could be attributed to the existence of ethanol in the growth process. It is proposed that during the preparation steps, the Zn ions are captured by the surface of ZnO due to the presence of ethanol which facilitates the agglomeration of ZnO nanocrystallites. These nanoparticles are tiny and unsteady; thus, they tend to form agglomerated ZnO by shooting with the laser. This is similar to the previously reported work. Schneider et al. reported that the size of the ZnO particles, morphology and aggregation of ZnO nanoparticles affected by the precursor and the surfactant [45]. It was reported that the agglomeration was due to the high surface energy of ZnO nanoparticles. In the laser irradiation process, the liquid is heated by laser pulse where long-pulse irradiation produces a higher temperature. Mintcheva, et al. reported that the temperature of the liquid media was affected by the width of the laser pulse. The ZnO nanoparticles were prepared using millisecond and nanosecond laser, to have temperatures of 80–83 °C and 25–27 °C, respectively [46]. These structures are important for photocatalysts application, due to the presence of nonporous and microporous which exhibited high surface area.

Figure 3c shows the morphology of sample EGZn examined by SEM. ZnO nanostructures exhibited nanospherical morphology. The microscopic images illustrate that the nanospheres growth densely with the lowest porosity than other samples as it is clearly shown in Fig. 3f. Therefore, there is a significant effect of ethylene glycol on the growth and morphology of sample EGZn. Sample EGZn exhibited a wide spreading of aggregated nanocrystallites ranging from ~ 40 to 80 nm ± 3 nm as in the schematic representation shown in Fig. 3i. Nevertheless, sample EGZn has monodisperse distribution due to its fatty nature, which capped the ZnO and slowed down the laser pulses and thus prevents the agglomeration and aggregation into larger structures. It's well known that both ethanol and ethylene glycol have comparable chemical structures while in the case of DI water the chemical structure is quite different which may explain the growth of sample DIZn in (1D).

These results are in good agreement with previous results. Recently, Ekaterina et al. prepared ZnO using LAL method through ablation of Zn metal by nanosecond laser in water and air environments [47]. They reported that when the ablation process was taking place in air spherical nanoparticles were obtained. However, when water was used as a liquid

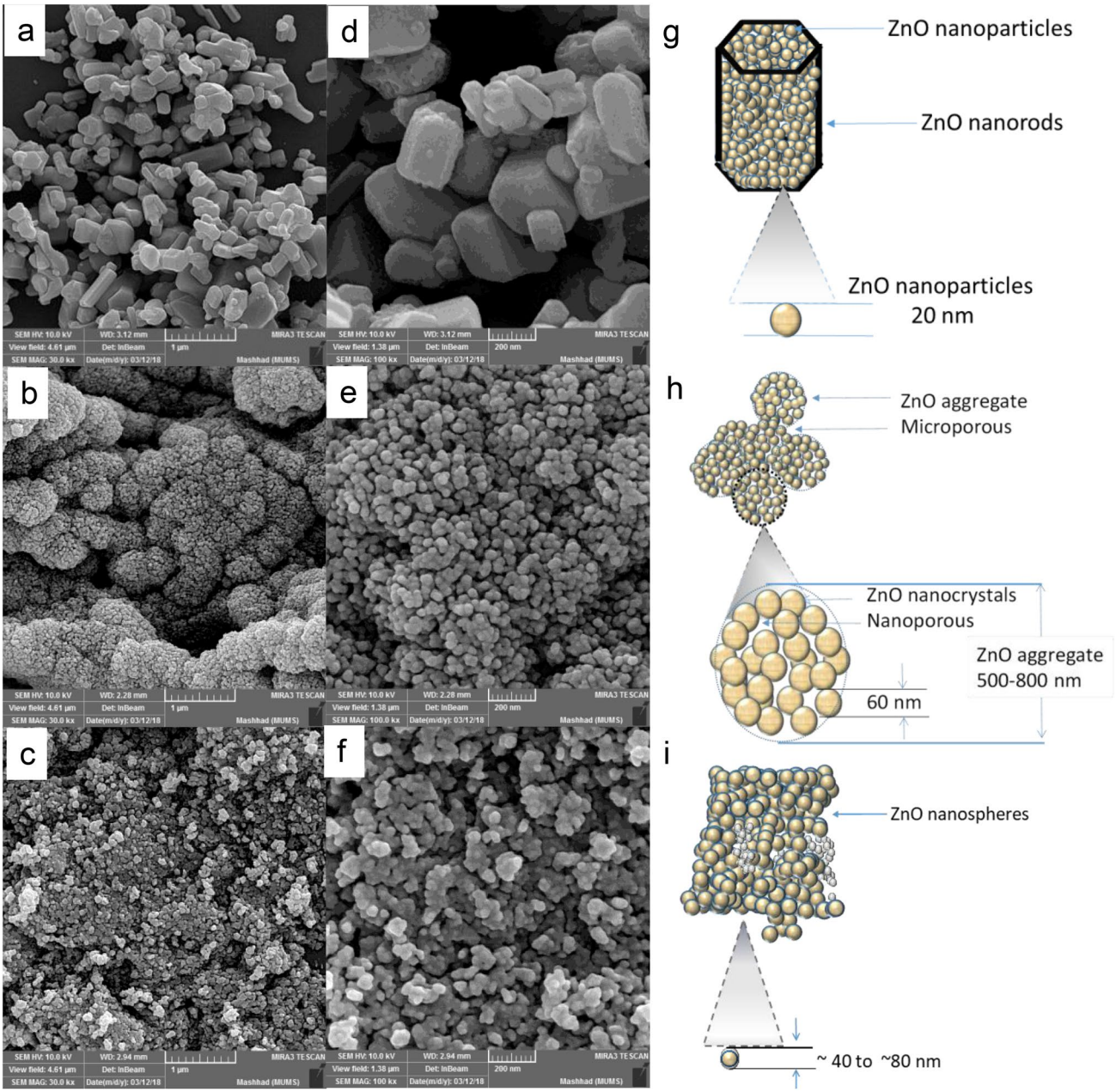

Fig. 3 Morphology of samples **a** DIZn, **b** EthZn, and **c** EGZn where the middle panel **d**, **e**, and **f** represents the high magnification. Meanwhile, **g**, **h**, and **i** represent the corresponding schematic graphs, respectively

media ZnO nanorods were synthesized. They found that the nanospheres had a larger surface area than the nanorods. Honda et al. reported that the irradiation of Zn metal in water with millisecond pulsed laser can produce ZnO nanorod [48]. They explained the formation of nanorods due to the increment of temperature during laser irradiation process. Furthermore, it was reported by Ishikawa et al. that ZnO nanorods were obtained by ablating Zn metal in water using nanosecond pulsed laser [34]. Zhang et al. reported in their previous studies that the elevated temperature and high pressure, which produced by laser radiation, act as a main factor during the pulsed laser irradiation in a liquid process [49]. Then, a plume would be produced that quickly cooled down in the solvent. Finally, nanoparticles would be obtained due to the agglomeration. As well, the morphology and particle sizes of nanoparticles are affected strongly by the pulse duration. Nevertheless, Ridha et al. prepared ZnO nanostructures by ablating the ZnO pellet using laser ablation in various liquids. They reported that the obtained nanostructures were grown as hexagonal nanosheets in DI

water while nanorods were prepared in ethanol and ethylene glycol [50]. Therefore, we can conclude that using the laser irradiation process, several parameters controlled the morphology of the prepared nanoparticles. These parameters could be the environment, the type of liquid, the width of the laser pulse, and the type of the target. The total surface area is inversely proportional to the size (radius) of nanoparticles; thus, the surface area of the smaller nanosphere is higher than the larger nanosphere. However, the nanorods exhibited a high aspect ratio (high surface to volume ratio) and a larger surface/volume ratio than nanospheres [51, 52].

3.3 EDX analysis

EDX characterizations were studied to analyze the composition of the samples. Figure 4 represents the EDX analysis of samples DIZn, EthZn, and EGZn. The figures confirm the presence of Zn and O elements on the Si substrate using the laser irradiation method. It is observed that the synthesized sample is pure ZnO due to the absence of other elements.

Figure 5a represents the UV-Vis absorption spectra of a colloidal suspension of samples (DIZn, EthZn, and EGZn). All the samples show a wide absorption range from 300 to 360 nm. The absorption edge is positioned at about 360 nm for ZnO, which is related to the typical electron transition from O 2p orbital to Zn 3d orbital. The shoulder which represents the highest absorption peak can be attributed to the essential electron transitions of ZnO from the valence band to the conduction band. The highest absorption edge of samples EGZn, DIZn, and EthZn is about (351.8 nm), (349.4 nm), and (348.3 nm), respectively. It was observed that the absorption maximum of the samples was blue-shifted. The highest absorption obtained when ethylene glycol was used to prepare the sample. This is due to the morphology of the sample EGZn which is characterized by small nanostructures and low porosity. The small nanoparticles dispersed well in the solution and absorbed more than 60% of the incident beam and thus prohibited the light to pass through them. The lowest absorption exhibited by microsphere (EthZn) due to its morphology is characterized by high porosity. Thus, it permits the light to penetrate it easily with a low portion of absorbance around 10%. The nanorods (DIZn) displayed middle absorbance ability due to their large size structure.

Figure 5b demonstrates the direct energy gap of samples EthZn, DIZn, and EGZn. It is noticed that the highest energy gap exhibited by sample EthZn, which is (3.59

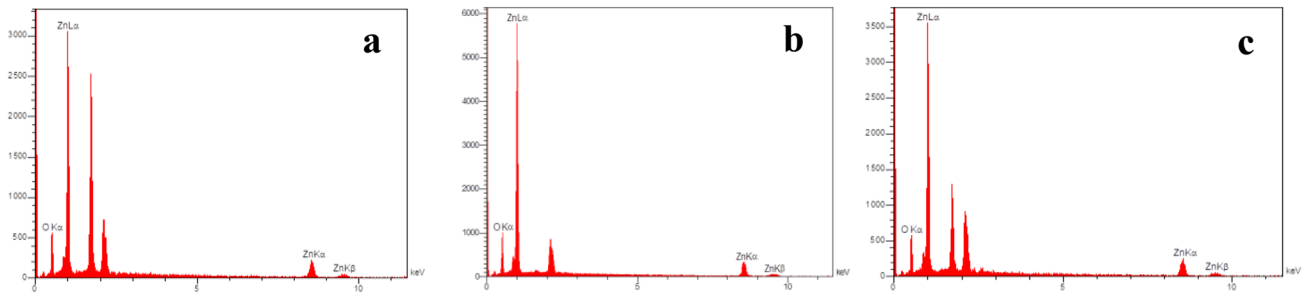

Fig. 4 EDX of ZnO samples **a** DIZn, **b** EthZn, and **c** EGZn prepared by LAL method at 6000 pulses and 180 mJ

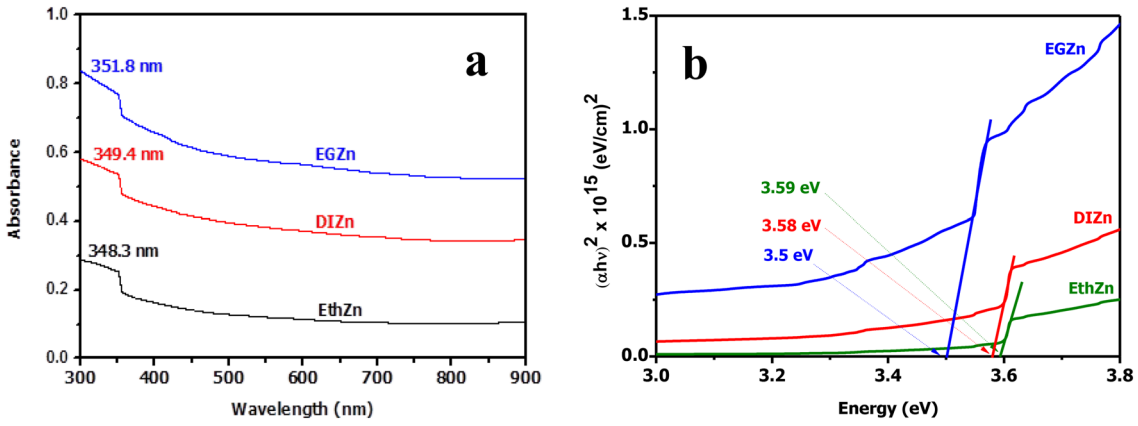

Fig. 5 Shows **a** the absorption spectra of the ZnO prepared in different solvents and **b** their corresponding Tauc plot for the direct bandgap of samples EthZn, DIZn, and EGZn

eV), reduced to (3.58 eV) of sample DIZn where the lowest value was (3.5 eV) of sample EGZn. The energy gap of the sample EthZn is greater than the energy gap of DIZn and EGZn. This could be attributed to the variances morphologies and particle size of the synthesized ZnO nanoparticles. These results are in good agreement with previously reported work. Comparing these results with previous work is worthy since there are several contradicts in these issues. Al-Nassar et al. prepared ZnO nanoparticles by the LAL method. They reported that as the laser pulse energy increased from 0.05 mJ and 1.11 mJ to 1.15 mJ, the size of nanoparticles increased [53]. This increment led to the red shifting of the absorption peaks. Khawla et al. prepared ZnO nanoparticles via irradiation zinc target in water for 10 min by 1064 nm nanosecond laser with frequency, pulse width, and energy equal to 10 Hz, 9 ns, and 80 mJ, respectively [54]. They reported that the prepared ZnO nanoparticles had a crystal size and a particle size equal to 20.97 and 56 nm, respectively, and exhibited energy gap equal to 3.29 eV. Hassoon et al., prepared ZnO nanostructures using laser irradiation in ethanol [55]. They studied the effect of several parameters such as laser energy and number of pulses on the energy gap of the prepared ZnO nanostructures. They reported that by increasing the laser energy from 500 to 900 mJ, the nanoparticles exhibited increment in their corresponding bandgap from 3.3 eV to 3.5 eV. They reported as well that the increment in the number of the laser pulses from 60 to 140 pulses led to raise the bandgap at the energy gap from 3.5 eV to 3.66 eV due to quantum confinement of smaller nanoparticles. Ismail et al. prepared ZnO nanoparticles via LAL method to ablate the metal zinc in water [56]. They found that as the laser fluence increased, both of the particle size and energy gap were increased as well. Anaraki et al. described the correlation of morphology and size with the optical bandgap of ZnO nanostructures [57]. They reported that the energy gap of nanorod morphology is 4.0 eV. By modifying the morphology to nanosheet the energy gap red shifted. Moghaddam et al. reported that ZnO nanostructures showed red shifting in the absorption edge which ascribed to the modifications in the morphology and particle size due to increments in irradiation time [58]. Meanwhile, the energy bandgap of the prepared ZnO nanostructures was decreased from 3.39 to 3.18 eV by extending the irradiation time from 12 to 36 h. Therefore, it is noticeable that the morphology of nanostructure controlled the energy gap.

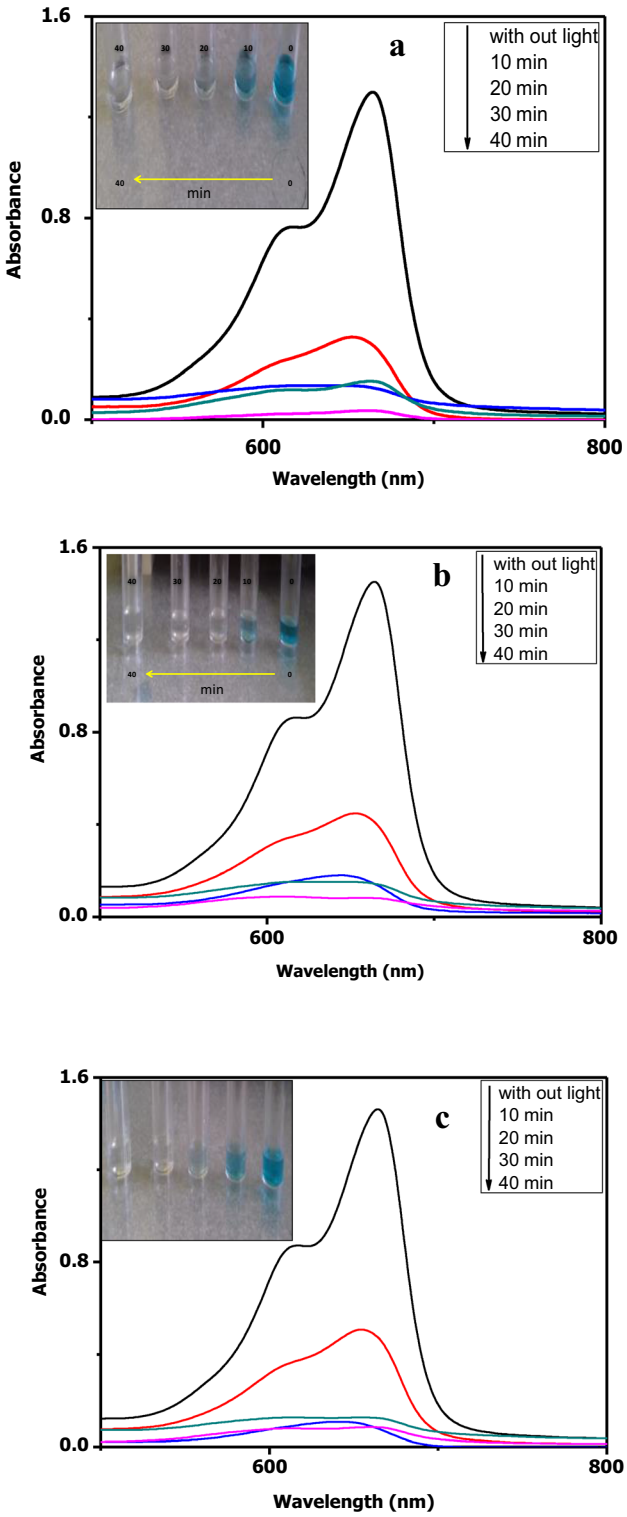

Fig. 6 UV–Visible absorption spectra of MB dye using ZnO where **a** DIZn, **b** EthZn, and **c** EGZn samples

3.4 Application of ZnO

Figure 6 explains the absorption spectra of MB dye before and after UV irradiation to study the removal activity by ZnO samples. Generally, all the prepared ZnO samples exhibit photocatalyst properties under ultraviolet light. As a good photocatalyst behavior, the MB spectra are systematically decreased with time, which indicates the degradation

of MB. This behavior occurs due to the fact that electron pairs are generated and migrated to the surface to form more hydroxyl radicals and thereby increase quantitative efficiency and catalytic efficiency [59].

It is observed from the Fig. 6a that using sample DIZn as a photocatalyst, the MB dye continues to degrade every (10 min) until it completely vanishes after (40 min). The noticed disorder between 20 and 30 min is due to the presence of very small ZnO nanoparticles that can't be separated by the centrifuge. Figure 6b exposes the absorption spectrum of MB dye in sample EthZn, where the gradual degradation of MB is observed as a function of time. The Figure displays a disorder in the sample EthZn at (20 to 30 min) due to the presence of ZnO nanoparticles stuck in the MB dye that cannot be separated by centrifuging and thus affect the absorption spectrum of the MB dye. Figure 6c shows the spectrum of MB dye absorption at the ethylene glycol, the gradual degradation of the MB dye is observed until the MB dye completely disappears. The degradation occurs faster using ZnO nanorods as a catalyst due to increased active surfaces and high surface area.

Figure 7 shows the effect of different ZnO samples prepared in various solvents used in the degradation of MB. The figure illustrates that the ZnO nanorods exhibited the highest photocatalyst activity. This is due to the ability of nanorods to transport the electrons faster than other structures. This is due to quantum confinement which improves transportation in only one free path. In addition, surface defects usually play an important role in the determination of photocatalysts' efficiency. As mentioned before, the crystalline defects of ZnO nanoparticles are mainly in the form of vacancies [59]. It is believed that the ZnO principally has exposed an active O^{2-} on (101), (002), and (110) facets. Therefore, these facets are deliberated as an active center for degradation.

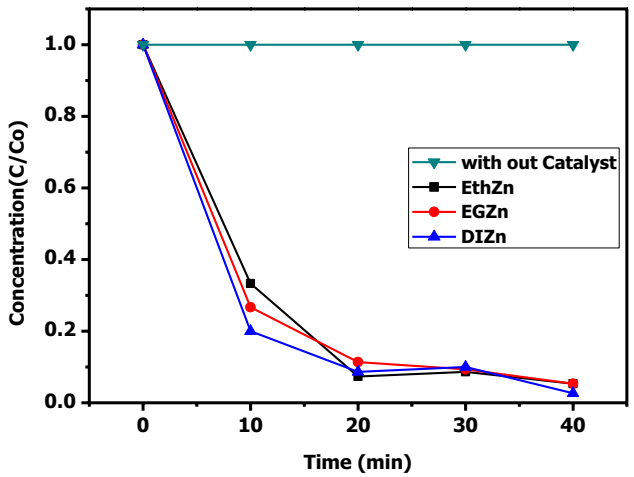

Fig. 7 Concentration spectra of MB using ZnO nanostructures as a catalyst

Accordingly, the presence of defects will increase the activity of photocatalysts degradation. The observed enhancement of the photocatalytic activity of ZnO nanorods (DIZn) could be attributed to the high surface area, which increases the opportunity to trap photons; therefore, more charge carriers would be generated.

Recently, several investigations reported the effects of the morphology of ZnO nanostructures on their photocatalytic activities. Zhang et al. reported that by increasing the aspect ratio of ZnO nanorods more surface defects can be formed and thus higher photocatalytic performance may be achieved [60]. Han et al. reported in their work that the photocatalytic activity of ZnO nanostructures is controlled by the chemisorption ability of the reacted surfaces [61]. Guo et al. reported that the photocatalytic activity of ZnO nanostructures depends mainly on the morphology. They found that the prepared ZnO nanoparticles exhibited smaller particle size and higher surface area than the ZnO tetrapods. Nevertheless, the ZnO tetrapods showed higher photocatalytic performance [62]. Mintcheva et al. prepared ZnO nanoparticles using LAL method. They revealed that the ZnO nanorods prepared with millisecond laser exhibited higher photocatalytic performance than the nanospherical that was prepared using (nanosecond laser) due to higher oxygen defects [46].

These obtained results evidently show that the morphology of the ZnO nanoparticles strongly depends on the type of liquid media. It was found that the prepared ZnO through irradiating zinc acetate by laser in DI water exhibited nanorod structures with higher catalyst activity compared to thus of ethanol or ethylene glycol.

The specific effects of using laser irradiation to prepare ZnO nanoparticles for photocatalyst degradation require further studies by intensively investigate the formed environments during the reactions. We suggested that another salts such as zinc nitrate as well as other liquids such as methanol, acetone, and benzyl alcohol have to be investigated as future work. The effect of various parameters such as temperature, pH, the intensity of light, dose of catalyst, and the concentration of dye still needs to be considered for future photocatalyst studies.

3.5 Photocatalysis mechanism

The photocatalysis is the process that accelerating increases the reaction rate by reducing the required activation energy. It also increases the rate of transformation of reactive materials without being change or consumption [63]. Thus, photocatalysis is an interaction in which light is used as an energizer for a material that will increase the rate of a chemical reaction without having a role in the reaction as shown in Fig. 8.

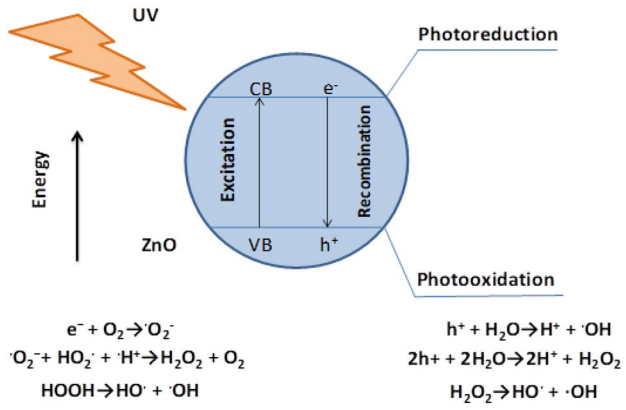

Fig. 8 Mechanism of ZnO as a photocatalysis material

The mechanism of the photocatalysis can be interpreted depending on the transitions of the electrons. When the ZnO nanocatalyst absorbs ultraviolet radiation, the electron moves from the valence band to the conductive band (Eq. 1). The electron in the conductive band may form organic peroxide or a hydrogen peroxide (H_2O_2) in the presence of oxygen and organic molecule (Eqs. 2, 3, and 4). Also, hydrogen peroxide can be generated in another path (Eqs. 5 and 6). It can form hydroxyl radicals (OH.), which are powerful oxidizing agents (Eq. 7). Producing roots are able to attack dye molecules and their degradation continues as long as the light is available (Eqs. 8 and 9) [64].

$$\mathrm{ZnO} + h\nu \rightarrow \left(\mathrm{e}_{\mathrm{CB}}^{-} + h_{\mathrm{VB}}^{+}\right) \quad (1)$$

$$\mathrm{e}_{\mathrm{CB}}^{-} + \mathrm{O}_2 \rightarrow \mathrm{O}_2^{\bullet -} \quad (2)$$

$$\mathrm{H_2O} + \mathrm{O}_2^{\bullet -} \rightarrow \mathrm{OOH}^{\bullet} + \mathrm{OH}^{-} \quad (3)$$

$$2\mathrm{OOH}^{\bullet} \rightarrow \mathrm{O_2} + \mathrm{H_2O_2} \quad (4)$$

$$\mathrm{O}_2^{\bullet -} + \mathrm{dye} \rightarrow \mathrm{dye} - \mathrm{OO}^{\bullet} \quad (5)$$

$$\mathrm{OOH}^{\bullet} + \mathrm{H_2O} + \mathrm{e}_{\mathrm{CB}}^{-} \rightarrow \mathrm{H_2O_2} + \mathrm{OH}^{-} \quad (6)$$

$$\mathrm{H_2O_2} + \mathrm{e}_{\mathrm{CB}}^{-} \rightarrow \mathrm{OH}^{\bullet} + \mathrm{OH}^{-} \quad (7)$$

$$\mathrm{H_2O_2} + \mathrm{O}_2^{\bullet -} \rightarrow \mathrm{OH}^{\bullet} + \mathrm{OH}^{-} + \mathrm{O_2} \quad (8)$$

$$\mathrm{OH}^{\bullet}/\mathrm{O}_2^{\bullet -}/\mathrm{ZnO}^{\bullet +} + \mathrm{dye} \rightarrow \mathrm{Dye\ degradation} \quad (9)$$

4 Conclusions

In the present study, we applied novel method to synthesis ZnO nanoparticles via irradiating $Zn(OCOCH_3)_2$ with laser in liquid. The effects of liquids variation (deionized (DI) water, ethanol, and ethylene glycol) on the properties of ZnO nanostructures were investigated. XRD results revealed that all the prepared ZnO nanostructures exhibited well crystalline hexagonal structure. The morphology of the synthesized ZnO exhibited the nanorod structures upon the incorporation of DI water in contrast to the ZnO growth into nanospheres when prepared in ethanol or ethylene glycol. The prepared samples were used as photocatalysts in degradation of MB dye. It was concluded that the best degradation of MB was obtained using ZnO nanorods as a catalyst. This is due to the enhancement of the active surfaces provided by nanorods.

Acknowledgements The authors would like to thank and appreciate Kerbala University for the support and assistance to this project.

References

1. F. Alosfur, M.H. Jumali, S. Radiman, N.J. Ridha, M.A. Yarmo, A.A. Umar, Visible light-responsive TiO_2 coated MWCNTs as a hybrid nanocatalysts. Int. J. Electrochem. Sci. **8**, 2977–2982 (2013)
2. F.K.M. Alosfur, M.H. Jumali, S. Radiman, N.J. Ridha, A.A. Umar, Visible light photocatalytic activity of TiO2/MWCNTs nanocomposite prepared using modified microwave technique, sensing technology (ICST), in *2013 Seventh International Conference on Sensing Technology (ICST)* (IEEE, Piscataway, 2013), pp. 777–781
3. C. Kolstad, *Intermediate environmental economics: international edition, OUP catalogue* (Oxford University Press, Oxford, 2011)
4. A. Balouch, M. Kolachi, F.N. Talpur, H. Khan, M.I. Bhanger, Sorption kinetics, isotherm and thermodynamic modeling of defluoridation of ground water using natural adsorbents. Am. J. Anal. Chem. **4**, 221 (2013)
5. M. Sudha, A. Saranya, G. Selvakumar, N. Sivakumar, Microbial degradation of azo dyes: a review. Int. J. Curr. Microb. Appl. Sci. **3**, 670–690 (2014)
6. F.K.M. Alosfur, M.H.H. Jumali, S. Radiman, N.J. Ridha, M.A. Yarmo, A.A. Umar, Modified microwave method for the synthesis of visible light-responsive TiO_2/MWCNTs nanocatalysts. Nanoscale Res. Lett. **8**, 346 (2013)
7. M.H.H. Jumali, F.K.M. Alosfur, S. Radiman, N.J. Ridha, M.A. Yarmo, A.A. Umar, Rapid synthesis of TiO_2/MWCNTs nanocatalyst with enhanced photocatalytic activity using modified microwave technique. Mater. Sci. Semicond. Process. **25**, 207–210 (2014)
8. S. Balu, K. Uma, G.-T. Pan, T. Yang, S. Ramaraj, Degradation of methylene blue dye in the presence of visible light using SiO_2@ α-Fe_2O_3 nanocomposites deposited on SnS_2 flowers. Materials **11**, 1030 (2018)
9. R. Karthik, R. Muthezhilan, A. Jaffar Hussain, K. Ramalingam, V. Rekha, Effective removal of Methylene Blue dye from water using three different low-cost adsorbents. Desalin. Water Treat. **57**, 10626–10631 (2016)

10. M. Punzi, *Treatment of Textile Wastewater by Combining Biological Processes and Advanced Oxidation* (Department of Biotechnology, Lund University, Lund, 2015)
11. F.K.M. Alosfur, N.J. Ridha, M.H.H. Jumali, S. Radiman, One-step formation of TiO_2 hollow spheres via a facile microwave-assisted process for photocatalytic activity. Nanotechnology **29**, 145707 (2018)
12. M. Safdar, Y. Junejo, A. Balouch, Efficient degradation of organic dyes by heterogeneous cefdinir derived silver nanocatalyst. J. Ind. Eng. Chem. **31**, 216–222 (2015)
13. A.A. Ouda, F.K.M. Alosfur, N.J. Ridha, S.H. Abud, N.M. Umran, H.H. Al-aaraji, R.A. Madlool, Facile method to synthesis of anatase TiO2 nanorods, in *Journal of physics: conference series*. (IOP Publishing, Bristol, 2018), p. 012038
14. T. Mahardika, N.A. Putri, A.E. Putri, V. Fauzia, L. Roza, I. Sugihartono, Y. Herbani, Rapid and low temperature synthesis of Ag nanoparticles on the ZnO nanorods for photocatalytic activity improvement. Results Phys. **13**, 102209 (2019)
15. Y.L. Pang, A.Z. Abdullah, S. Bhatia, Review on sonochemical methods in the presence of catalysts and chemical additives for treatment of organic pollutants in wastewater. Desalination **277**, 1–14 (2011)
16. Y. Deng, R. Zhao, Advanced oxidation processes (AOPs) in wastewater treatment. Curr. Pollut. Rep. **1**, 167–176 (2015)
17. C.B. Ong, L.Y. Ng, A.W. Mohammad, A review of ZnO nanoparticles as solar photocatalysts: synthesis, mechanisms and applications. Renew. Sustain. Energy Rev. **81**, 536–551 (2018)
18. Z.A. Hussein, S.K. Abbas, L.M. Ahmed, *UV-A Activated ZrO_2 via Photodecolorization of Methyl Green Dye, IOP Conference Series: Materials Science and Engineering* (IOP Publishing, Bristol, 2018), p. 012132
19. L.M. Ahmed, S.I. Saaed, A.A. Marhoon, Effect of oxidation agents on photo-decolorization of vitamin B 12 in the presence of ZnO/UV-A system. Indones. J. Chem. **18**, 272–278 (2018)
20. K.M. Reza, A. Kurny, F. Gulshan, Parameters affecting the photocatalytic degradation of dyes using TiO_2: a review. Appl. Water Sci. **7**, 1569–1578 (2017)
21. M.H.H. Jumali, F.K.M. Alosfur, S. Radiman, A.A. Umar, Dressing of MWCNTs with TiO_2 nanoparticles using modified microwave method, in *Advanced materials research* (Trans Tech Publications, Stäfa, 2012), pp. 228–231
22. F.K.M. Alosfur, A.A. Ouda, N.J. Ridha, S.H. Abud, Structure and optical properties of TiO_2 nanorods prepared using polyol solvothermal method, in *AIP conference proceedings* (AIP Publishing, College Park, 2019), p. 030025
23. F.K.M. Alosfur, A.A. Ouda, N.J. Ridha, S.H. Abud, High photocatalytic activity of TiO_2 nanorods prepared by simple method. Mater. Res. Exp. **6**, 065028 (2019)
24. M.H.H. Jumali, N.J. Ridha, A.A. Umar, M. Yahya, M.M. Salleh, Characterization of SnO_2 nanoparticles prepared by two different wet chemistry methods, in *Advance materials research* (Trans Tech Publications, Stäfa, 2012), pp. 322–326
25. H.F. Oleiwi, H. Al-Taay, S.Y. Al-Ani, K.J. Tahir, Structural and optical properties of Al_2O_3 nanocrystalline: effect of deposition time, in *AIP conference proceedings* (AIP Publishing LLC, Melville, 2019), p. 030027
26. N.J. Ridha, M.H.H. Jumali, A.A. Umar, F. Alosfur, Defects-controlled ZnO nanorods with high aspect ratio for ethanol detection. Int. J. Electrochem. Sci. **8**, 4583–4594 (2013)
27. N.J. Ridha, F.K.M. Alosfur, M.H.H. Jumali, S. Radiman, Dimensional effect of ZnO nanorods on gas-sensing performance. J. Phys. D: Appl. Phys. **51**, 435101 (2018)
28. M.Y.A. Rahman, A. Umar, R. Taslim, M.M. Salleh, Effect of surfactant on the physical properties of ZnO nanorods and the performance of ZnO photoelectrochemical cell. J. Exp. Nanosci. **10**, 599–609 (2015)
29. L.M. Ahmed, M. Jassim, M. Mohammed, D. Hamza, Advanced oxidation processes for carmoisine (E122) dye in UVA/ZnO system: Influencing pH, temperature and oxidant agents on dye solution. J. Glob. Pharm. Technol. **10**, 248–254 (2018)
30. M.M. Radhi, F.K.M. Alosfur, N.J. Ridha, Voltammetric characterization of grafted polymer modified with ZnO nanoparticles on glassy carbon electrode. Russ. J. Electrochem. **54**, 27–32 (2018)
31. N.A. Nema, A. Jassim, O.K. Abdali, S. Kahdum, A.O. Mousa, Modification of photocatalytic activity of zinc oxide photocatalyst by sensitization with riboflavin as a photosensitizer. World Sci. News **22**, 40–50 (2015)
32. N.M. Umran, H.A. Rashed, F.K.M. Alosfura, N.J. Ridha, Effect of Substitution (Al and P) Atoms in ZnO Nanosheet on Structural and Electronic Properties, J. Phys. Conf. Ser., **1032**, p. 012045 (2018)
33. H.A. Rashed, N.M. Umran, The stability and electronic properties of Si-doped ZnO nanosheet: a DFT study. Mater. Res. Exp., **6**,045044(2018)
34. Y. Ishikawa, Y. Shimizu, T. Sasaki, N. Koshizaki, Preparation of zinc oxide nanorods using pulsed laser ablation in water media at high temperature. J. Colloid Interface Sci. **300**, 612–615 (2006)
35. N.J. Ridha, H.B.A. Kadhim, F.K.M. Alosfur, L.H. Abood, R. Madlol, *AIP Conference Proceedings* (AIP Publishing, College Park, 2019), p. 030026
36. K.K. Lee, D. Wang, O. Shinobu, T. Ohshima, Reliability of gamma-irradiated n-channel ZnO thin-film transistors: electronic and interface properties. Radiat. Eff. Defects Solids **173**, 250–260 (2018)
37. R.A.A. Madlol, Structural and optical properties of ZnO nanotube synthesis via novel method. Results Phys. **7**, 1498–1503 (2017)
38. N.J. Ridha, A.A. Umar, F. Alosfur, M.H.H. Jumali, M.M. Salleh, Microwave assisted hydrothermal method for porous zinc oxide nanostructured-films. J. Nanosci. Nanotechnol. **13**, 2667–2674 (2013)
39. N.J. Ridha, M.H.H. Jumali, A.A. Umar, F.K. Mohamad, *Ethanol Sensor Based on ZnO Nanostructures Prepared via Microwave Oven, Sensing Technology (ICST)* (IEEE, Piscataway, 2013), pp. 121–126
40. Y. Cai, X. Luo, M. Maclean, Y. Qin, M. Duxbury, F. Ding, A single-step fabrication approach for development of antimicrobial surfaces. J. Mater. Process. Technol. **271**, 249–260 (2019)
41. H.B.A. Kadhim, N.J. Ridha, F.K.M. Alosfur, N.M. Umran, R. Madlol, K.J. Tahir, R.T. Ahmed, Ablation of ZnO in liquid by nanosecond laser. J. Phys. Conf. Ser. **1032**, p. 012039
42. A.M. Brito-Silva, L.A. Gómez, C.B. De Araújo, A. Galembeck, Laser ablated silver nanoparticles with nearly the same size in different carrier media. J. Nanomater. **2010**, 10 (2010)
43. A. Pyatenko, K. Shimokawa, M. Yamaguchi, O. Nishimura, M. Suzuki, Synthesis of silver nanoparticles by laser ablation in pure water. Appl. Phys. A **79**, 803–806 (2004)
44. S.K. Abass, J.A. Al-Hilfi, S.K. Abbas, L.M. Ahmed, Preparation, characterization and study the photodecolorization of mixed-ligand binuclear Co (II) complex of Schiff base by ZnO. Indon. J. Chem. **20**, 404–412 (2020)
45. J.r.J. Schneider, R.C. Hoffmann, J.r. Engstler, A. Klyszcz, E. Erdem, P. Jakes, R.d.-A. Eichel, L. Pitta-Bauermann, J. Bill, Synthesis, characterization, defect chemistry, and FET properties of microwave-derived nanoscaled zinc oxide. Chem. Mater. **22**, 2203–2212 (2010)
46. N. Mintcheva, A. Aljulaih, W. Wunderlich, S. Kulinich, S. Iwamori, Laser-ablated ZnO nanoparticles and their photocatalytic activity toward organic pollutants. Materials **11**, 1127 (2018)
47. E.A. Gavrilenko, D.A. Goncharova, I.N. Lapin, A.L. Nemoykina, V.A. Svetlichnyi, A.A. Aljulaih, N. Mintcheva, S.A. Kulinich, Comparative study of physicochemical and antibacterial

properties of ZnO nanoparticles prepared by laser ablation of Zn target in water and air. Materials **12**, 186 (2019)
48. M. Honda, T. Goto, T. Owashi, A.G. Rozhin, S. Yamaguchi, T. Ito, S.A. Kulinich, ZnO nanorods prepared via ablation of Zn with millisecond laser in liquid media. Phys. Chem. Chem. Phys. **18**, 23628–23637 (2016)
49. K. Zhang, D.S. Ivanov, R.A. Ganeev, G.S. Boltaev, P.S. Krishnendu, S.C. Singh, M.E. Garcia, I.N. Zavestovskaya, C. Guo, Pulse Duration and Wavelength Effects of Laser Ablation on the Oxidation, Hydrolysis, and Aging of Aluminum Nanoparticles in Water. Nanomaterials **9**, 767 (2019)
50. N.J. Ridha, H.B.A. Kadhim, F.K.M. Alosfur, R.T. Ahmed, ZnO nanofluids prepared by laser ablation in various solvents. Mater. Res. Exp. **5**, 125008 (2018)
51. J.H. Park, G. von Maltzahn, L. Zhang, A.M. Derfus, D. Simberg, T.J. Harris, E. Ruoslahti, S.N. Bhatia, M.J. Sailor, Systematic surface engineering of magnetic nanoworms for in vivo tumor targeting. Small **5**, 694–700 (2009)
52. V.P. Chauhan, Z. Popović, O. Chen, J. Cui, D. Fukumura, M.G. Bawendi, R.K. Jain, Fluorescent nanorods and nanospheres for real-time in vivo probing of nanoparticle shape-dependent tumor penetration. Angew. Chem. Int. Ed. **50**, 11417–11420 (2011)
53. S.I. Al-Nassar, F.I. Hussein, The effect of laser pulse energy on ZnO nanoparticles formation by liquid phase pulsed laser ablation. J. Mater. Res. Technol. **8**, 4026–4031 (2019)
54. K.S. Khashan, M. Mahdi, Preparation of indium-doped zinc oxide nanoparticles by pulsed laser ablation in liquid technique and their characterization. Appl. Nanosci. **7**, 589–596 (2017)
55. K.I. Hassoon, S.H. Sabeeh, M.A. Khalaf, ZnO nano particles (NPs) properties prepared by liquid phase laser ablation (LPLA). J. Al-Nahrain Univ.-Sci. **20**, 70–77 (2017)
56. R.A. Ismail, A.K. Ali, M.M. Ismail, K.I. Hassoon, Preparation and characterization of colloidal ZnO nanoparticles using nanosecond laser ablation in water. Appl. Nanosci. **1**, 45–49 (2011)
57. A.A. Firooz, R.A. Mirzaie, F. Kamrani, Effect of morphological ZnO nanostructures on the optical and decolorization properties. J. Struct. Chem. **59**, 739–743 (2018)
58. A.B. Moghaddam, M. Moniri, S. Azizi, R.A. Rahim, A.B. Ariff, W.Z. Saad, F. Namvar, M. Navaderi, R. Mohamad, Biosynthesis of ZnO nanoparticles by a new Pichia kudriavzevii yeast strain and evaluation of their antimicrobial and antioxidant activities. Molecules **22**, 872 (2017)
59. Q. Zhou, J.Z. Wen, P. Zhao, W.A. Anderson, Synthesis of vertically-aligned zinc oxide nanowires and their application as a photocatalyst. Nanomaterials **7**, 9 (2017)
60. X. Zhang, J. Qin, Y. Xue, P. Yu, B. Zhang, L. Wang, R. Liu, Effect of aspect ratio and surface defects on the photocatalytic activity of ZnO nanorods. Sci. Rep. **4**, 4596 (2014)
61. X.-G. Han, H.-Z. He, Q. Kuang, X. Zhou, X.-H. Zhang, T. Xu, Z.-X. Xie, L.-S. Zheng, Controlling morphologies and tuning the related properties of nano/microstructured ZnO crystallites. J. Phys. Chem. C **113**, 584–589 (2008)
62. M.Y. Guo, A.M.C. Ng, F. Liu, A.B. Djurisic, W.K. Chan, H. Su, K.S. Wong, Effect of native defects on photocatalytic properties of ZnO. J. Phys. Chem. C **115**, 11095–11101 (2011)
63. C.-W. Tang, Study of photocatalytic degradation of methyl orange on different morphologies of ZnO catalysts. Mod. Res. Catal. **2**, 19 (2013)
64. M.A. Johar, R.A. Afzal, A.A. Alazba, U. Manzoor, Photocatalysis and bandgap engineering using ZnO nanocomposites. Adv. Mater. Sci. Eng. **6**, 1–22 (2015)